

Solar Biomass Reforming and Hydrogen Production with Earth-Abundant Si-Based Photocatalysts

Yuri Choi, Sungho Choi, Inhui Lee, Trang Vu Thien Nguyen, Sanghyun Bae, Yong Hwan Kim, Jaegwon Ryu, Soojin Park,* and Jungki Ryu*

Efficient electrochemical hydrogen production and biomass refinery are crucial for the decarbonization of various sectors. However, their energy-intensive nature and low efficiency have hindered their practical application. In this study, earth-abundant and non-toxic photocatalysts that can produce hydrogen and reform biomass efficiently, utilizing unlimited solar energy, are presented. The approach involves using low-bandgap Si flakes (SiF) for efficient light-harvesting, followed by modification with Ni-coordinated N-doped graphene quantum dots (Ni-NGQDs) to enable efficient and stable light-driven biomass reforming and hydrogen production. When using kraft lignin as a model biomass, SiF/Ni-NQGDs facilitate record-high hydrogen productivity at $14.2 \text{ mmol g}_{\text{cat}}^{-1} \text{ h}^{-1}$ and vanillin yield of $147.1 \text{ mg g}_{\text{lignin}}^{-1}$ under simulated sunlight without any buffering agent and sacrificial electron donors. SiF/Ni-NQGDs can be readily recycled without any noticeable performance degradation owing to the prevention of deactivation of Si via oxidation. This strategy provides valuable insights into the efficient utilization of solar energy and practical applications of electro-synthesis and biomass refinement.

are crucial for sustainable chemical industries that rely heavily on fossil fuels.^[1,2] Currently, hydrogen and various platform chemicals are produced from fossil fuels with significant CO₂ emissions, highlighting the need for alternative production technologies.^[3] Consequently, there is growing interest from academia, industry, and governments in water electrolysis and biomass refinery owing to their abundant raw materials and carbon-neutral life cycles. They have been extensively investigated from the perspectives of catalyst development,^[4–6] process and reactor design,^[7–10] and techno-economic analysis.^[11,12] However, their practical implementation remains challenging due to various technological and economical hurdles. For instance, hydrogen production through water electrolysis is energy-intensive and reliant on expensive and unsustainable elements (e.g., Pt and Ir),^[4,13] primarily due to the slow

1. Introduction

Green hydrogen production via water electrolysis and the effective utilization of renewable carbon via biomass reforming

kinetics and high overpotential of water oxidation.^[14] Meanwhile, biomass refineries suffer from low energy efficiency, productivity, and selectivity, and require harsh processing conditions, particularly when using inhomogeneous and recalcitrant biomass

Y. Choi, I. Lee, T. V. T. Nguyen, S. Bae, Y. H. Kim, Jungki Ryu
School of Energy and Chemical Engineering
Ulsan National Institute of Science and Technology (UNIST)
Ulsan 44919, Republic of Korea
E-mail: jryu@unist.ac.kr

S. Choi, S. Park
Division of Advanced Materials Science
Pohang University of Science and Technology (POSTECH)
Pohang 37673, Republic of Korea
E-mail: soojin.park@postech.ac.kr


Y. H. Kim, Jungki Ryu
Graduate School of Carbon Neutrality
Ulsan National Institute of Science and Technology (UNIST)
Ulsan 44919, Republic of Korea

Jaegwon Ryu
Department of Chemical and Biomolecular Engineering
Sogang University
Seoul 04107, Republic of Korea

S. Park
Department of Chemistry
Pohang University of Science and Technology (POSTECH)
Pohang 37673, Republic of Korea

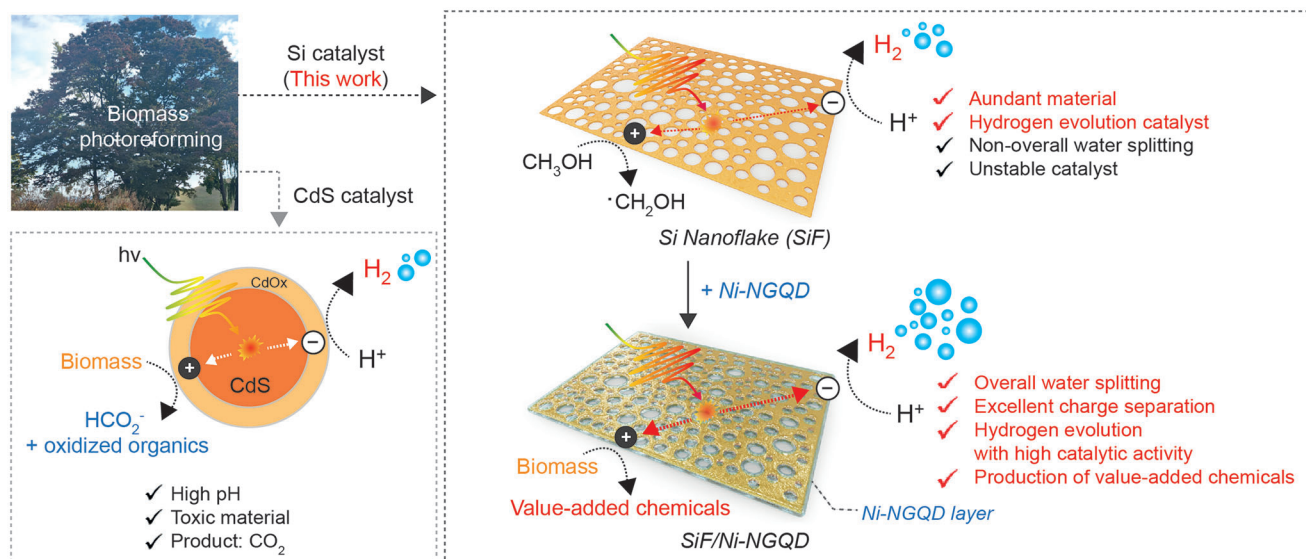
Jungki Ryu
Emergent Hydrogen Technology R&D Center
Ulsan National Institute of Science and Technology (UNIST)
Ulsan 44919, Republic of Korea

Jungki Ryu
Center for Renewable Carbon
Ulsan National Institute of Science and Technology (UNIST)
Ulsan 44919, Republic of Korea

 The ORCID identification number(s) for the author(s) of this article can be found under <https://doi.org/10.1002/adma.202301576>

© 2023 The Authors. Advanced Materials published by Wiley-VCH GmbH. This is an open access article under the terms of the Creative Commons Attribution License, which permits use, distribution and reproduction in any medium, provided the original work is properly cited.

DOI: 10.1002/adma.202301576



Scheme 1. Schematic illustration of the synthesis and application of SiF/Ni-NGQDs for efficient biomass reforming and hydrogen production under solar irradiation and mild conditions.

(e.g., lignin and lignocellulose) to avoid conflicts with the food supply.^[9,15,16]

Recent efforts have aimed to overcome these challenges by combining biomass reforming and hydrogen production with unlimited solar energy (i.e., biomass photo-reforming and hydrogen production). In principle, various biomass can be (photo)electrochemically depolymerized to produce valuable chemicals while supplying electrons and protons as an efficient alternative to water for hydrogen production.^[17–22] For example, conventional photocatalysts such as TiO₂ and CdS have been utilized for biomass photo-reforming and hydrogen production. These photocatalysts can oxidize or degrade biomass-derived chemicals such as glucose^[23,24] and 5-(hydroxymethyl)furfural^[125] to produce value-added chemicals. While these studies relied on edible or highly processed biomass-derived chemicals, Reiser et al. recently reported the utilization of non-edible biomass (e.g., cellulose and lignin) and visible-light-active CdS/CdO_x photocatalysts for hydrogen production under simulated solar irradiation.^[26] Despite promising results, these photocatalysts have critical limitations for practical applications, such as limited utilization of sunlight due to a large bandgap (2.4 eV for CdS and >3.2 eV for TiO₂), toxicity and photocorrosion (e.g., CdS),^[27,28] and harsh conditions (e.g., 10.0 M NaOH).^[26] Moreover, many studies have focused mostly on efficient solar hydrogen production and less on the selective production of biomass-derived chemicals, especially when using lignin. Although there was an interesting recent report about solar reforming of biomass under mild conditions (e.g., neutral pH) using non-toxic carbon dot photocatalysts, the efficiency of solar hydrogen production and biomass reforming is still unsatisfactory (e.g., 8.4 μmol H₂ for 24 h, which corresponds to ≈160 μmol g_{cat}⁻¹ h⁻¹) for practical application.^[29] In summary, there is still a lack of efficient, stable, and non-toxic photocatalysts for biomass photo-reforming with simultaneous production of hydrogen and valuable chemicals under mild conditions.

Herein, we report the synthesis of earth-abundant silicon-based photocatalysts (SiF/Ni-NGQD) for light-driven biomass reforming and hydrogen production by modifying porous silicon flake (SiF) with Ni-coordinated N-doped graphene quantum dots (Ni-NGQDs) (**Scheme 1**). Porous SiF is utilized for panchromatic visible light harvesting and photocatalytic hydrogen evolution reaction (HER), and subsequently modified with Ni-NGQDs for oxidative biomass reforming. Our systematic analyses indicate that Ni-NGQDs improve the efficiencies of the charge separation/transfer and selective oxidative reforming of biomass (e.g., lignin, cellulose, and hemicellulose) due to their graphitic structure, abundant functional groups, and Ni-active site. As a result, SiF/Ni-NGQD enables efficient photo-reforming of biomass with concurrent hydrogen production. Using lignin as an electron source, the SiF/Ni-NGQD produces hydrogen at 14.2 mmol g_{cat}⁻¹ h⁻¹ and vanillin at 147.1 mg g_{lignin}⁻¹ under simulated sunlight without any buffering agent and sacrificial electron donors. To the best of our knowledge, this is the first report about simultaneous photocatalytic production of hydrogen and selective value-added chemicals from lignin under mild conditions at pH 7.0 without the use of strongly acidic or alkaline solutions. Moreover, SiF/Ni-NGQD photocatalysts can be readily recycled without noticeable performance degradation owing to the protective role of Ni-NGQDs against the oxidation of SiF. This approach provides valuable insights into the design of hybrid photocatalysts for efficient hydrogen production and biomass photo-reforming.

2. Results and Discussion

We chose SiF as a photocatalyst for solar biomass reforming and hydrogen production. Although SiF has a narrow bandgap (1.7 eV) for broad light harvesting, suitable conduction band edge position for HER, and inherent HER activity without cocatalysts, it has critical limitations for practical applications, such as easy surface oxidation and low stability in aqueous solution, as well as

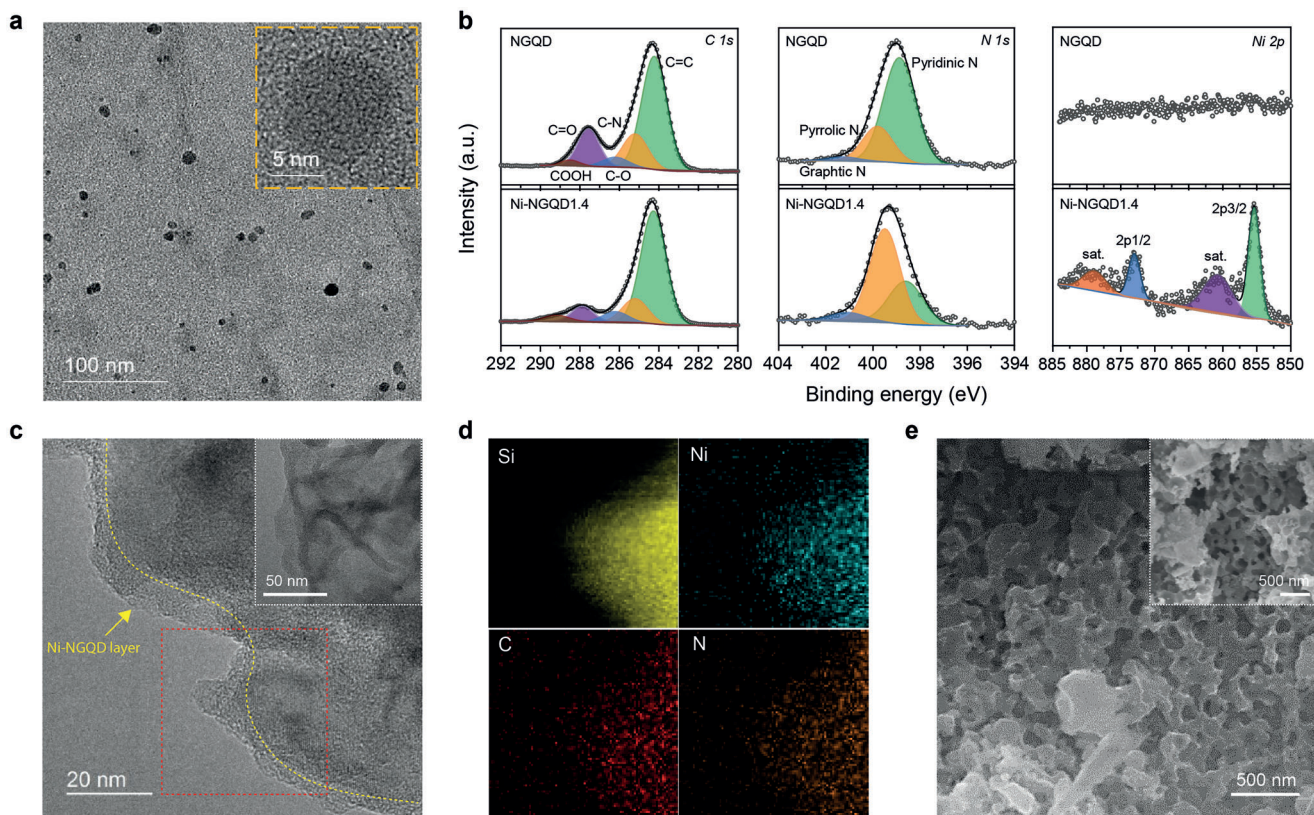


Figure 1. Characterization of as-synthesized Ni-NGQDs and SiF/Ni-NGQDs. a) TEM image of Ni-NGQD1.4. The inset shows a high-resolution TEM image of Ni-NGQD1.4. b) High-resolution C 1s, N 1s, and Ni 2p XPS spectra of NGQDs and Ni-NGQD1.4. c) TEM and d) elemental mapping images of SiF/Ni-NGQD1.4. e) SEM image of SiF/Ni-NGQD1.4. The inset images in Figures (c) and (e) show the morphology of the pristine SiF.

low catalytic activity and selectivity for oxidative biomass reforming. To address these issues, we modified SiF with Ni-NGQDs, which are expected to serve multifunctional roles by preventing surface oxidation, enhancing charge separation, and boosting catalytic activity for oxidative biomass reforming. Among various NGQDs with different metal ions, we selected Ni-NGQDs because Ni-based compounds are frequently utilized for catalytic biomass reforming.^[30] Ni-NGQDs were synthesized through a hydrothermal reaction with tannic acid, ethylenediamine, and varying amounts of NiCl₂. It is noted that the suffix numbers represent the relative amounts (wt.%) of NiCl₂ for the synthesis of Ni-NGQDs. Metal-free NGQDs were also prepared as a control.^[31]

As-synthesized NGQDs and Ni-NGQDs were characterized by various methods. According to transmission electron microscopy (TEM) and size distribution analysis, NGQDs and Ni-NGQDs were ≈ 11 nm in diameter (Figure 1a; Figure S1, Supporting Information). Metal-free NGQDs exhibited a strong absorption peak at 260 nm due to sp²-hybridized carbon and a shoulder peak at ≈ 400 nm due to surface states (Figure S2, Supporting Information). Compared to NGQDs, the Ni-NGQDs had an additional peak at 273 nm and a weaker shoulder peak due to the formation of metal-to-ligand charge transfer complex and the passivation of surface states, respectively.^[32] These can be beneficial for the separation and transfer of photoexcited electrons and holes for efficient photocatalysis.^[33] Inductively coupled plasma opti-

cal emission spectroscopy (ICP-OES) showed that the Ni contents in Ni-NGQDs were precisely controlled and proportional to the Ni contents in the precursor solutions (Table S1, Supporting Information). The formation of N-doped graphitic carbon for both NGQDs and Ni-NGQDs and atomic dispersion of Ni ions in Ni-NGQDs were confirmed by X-ray photoelectron spectroscopy (XPS). The high-resolution C 1s and N 1s XPS spectra showed a higher population of sp² C, graphitic N, and pyrrolic N configurations in the Ni-NGQDs than in the NGQDs (Figure 1b; Figure S3, Supporting Information). According to the literature, the formation of pyrrolic complexes is thermodynamically more favorable than pyridinic complexes for the synthesis of Ni-coordinated carbon structure.^[34] The Ni-NGQDs exhibited a Ni 2p_{3/2} peak at 855.0 eV and no Ni⁰ peak at ≈ 853.2 eV (Figure S4, Supporting Information).^[35] Satellite peaks of Ni 2p_{3/2} and Ni 2p_{1/2} were clearly observed with the increase in the amounts of Ni in the Ni-NGQDs (Figure 1b; Figure S4, Supporting Information). X-ray diffraction (XRD) analysis showed no sign of crystalline Ni (Figure S5, Supporting Information). It is noteworthy that there was a red shift of the pyrrolic N peaks when Ni was coordinated with NGQDs. All the results consistently suggest that in the Ni-NGQDs, Ni ^{$\delta+$} ions ($0 < \delta < 2$) rather than metallic Ni⁰ are atomically dispersed and form metal-to-ligand charge transfer complexes, beneficial for efficient photocatalysis.

Next, we prepared and characterized the SiF modified with Ni-NGQDs (SiF/Ni-NGQD) (Figure S6, Supporting Information).

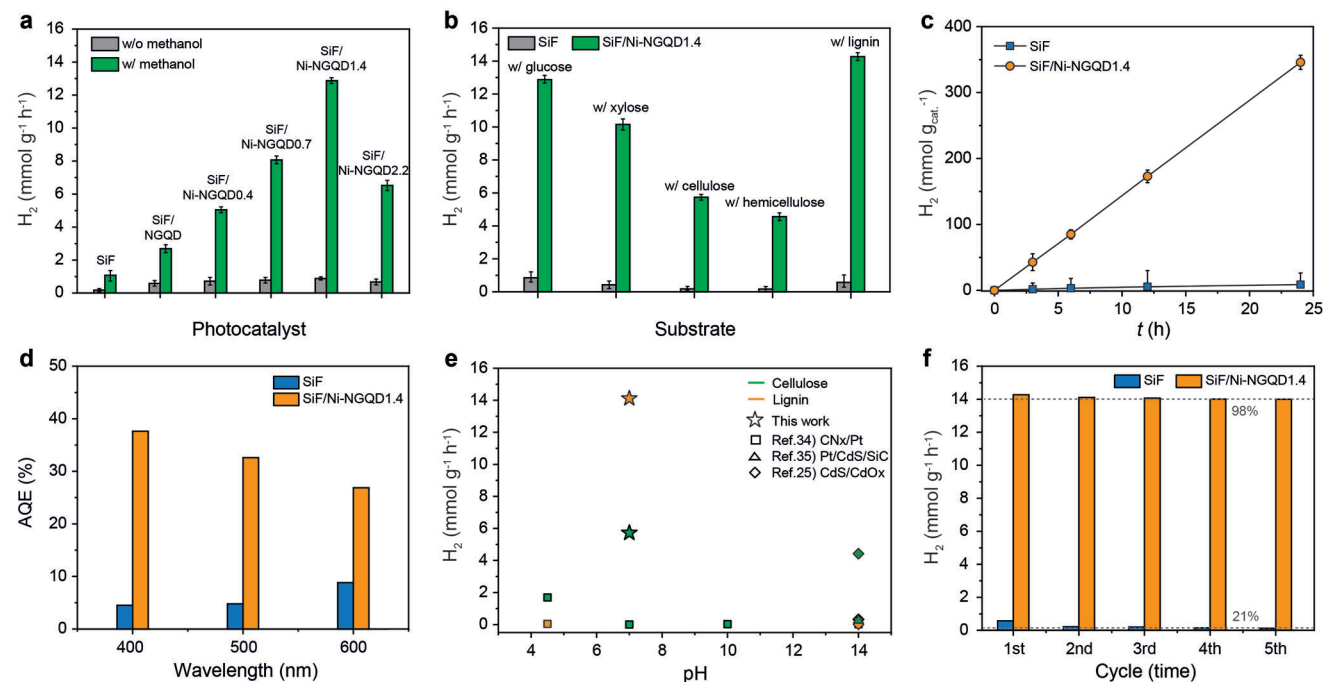


Figure 2. Photocatalytic hydrogen production by SiF/Ni-NGQDs. a) Effect of the decoration of SiF with Ni-NQDs, the Ni contents in Ni-NGQDs, and the use of methanol as a sacrificial electron donor on the photocatalytic hydrogen production. b) Photocatalytic hydrogen evolution using various biomasses, such as glucose, xylose, cellulose, hemicellulose, and lignin. c) Light-driven hydrogen evolution profiles with SiF and SiF/Ni-NGQD1.4 photocatalysts when using lignin. d) AQE of SiF and SiF/Ni-NGQD1.4 at 400, 500, and 600 nm. e) Comparison of the hydrogen production rate of our SiF/Ni-NGQD and other notable photocatalysts for light-driven hydrogen production and biomass reforming. f) Recyclability test of the SiF and the SiF/Ni-NGQD1.4 photocatalysts with lignin oxidation. The graphs contained the error bars.

The SiF was synthesized through magnesiothermic reduction and subsequent simple acid leaching process using natural talc clay according to the literature^[36] (see the experimental section in detail) and coated with Ni-NGQDs via a simple mixing due to abundant, adhesive phenolic groups.^[31] TEM and elemental mapping analyses of the SiF/Ni-NGQD showed that 2.3 nm of a Ni-NGQD layer was uniformly coated on the surface of SiF (Figure 1c,d). Before and after the modification, there was negligible change in porous structure of SiF, as shown in scanning electron microscopy (SEM) and Brunauer–Emmett–Teller (BET) analyses (Figure 1e; Figure S7, Supporting Information). In addition, there was no difference between the intensity and shape of high-resolution Si 2p XPS spectra of SiF and SiF/Ni-NGQD (Figure S8, Supporting Information). Photophysical properties of the SiF and the SiF/Ni-NGQDs were investigated using diffuse reflectance and ultraviolet photoelectron spectroscopy (UPS). The SiF had a low bandgap of 1.71 eV with a conduction band edge position of -1.11 V versus standard hydrogen electrode (V_{SHE}) suitable for HER. The SiF's valence band edge position of 0.60 V_{SHE} was insufficient for oxygen evolution reactions (OER) but sufficient enough for the oxidation of alcohols and various biomass (Figure S9, Supporting Information). Although the NGQDs and the Ni-NGQDs themselves had a bandgap of ≈ 3.1 eV with visible light activity, their contribution to solar light harvesting was negligible due to their larger bandgap than SiF and low loading (Figure S10 and S11, Supporting Information).

Based on these findings, we investigated photocatalytic activity of SiF/Ni-NGQDs with varying amounts of Ni-loading for hy-

drogen production under simulated sunlight illumination with and without methanol as a sacrificial electron donor. Unbuffered aqueous solutions were used throughout the photocatalytic experiments. Of note, except for SiF, which showed a catalytic activity of 1.1 $\text{mmol g}^{-1} \text{h}^{-1}$, the NGQDs or the Ni-NGQDs alone exhibited low photocatalytic activity even in the presence of methanol (Figure S12, Supporting Information). No or negligible activity was observed in the absence of methanol. The non-zero activity of SiF, even without methanol, may be attributed to the extraction of electrons via self-oxidation (i.e., self-destruction), as reported previously.^[36] The photocatalytic activity of SiF was dramatically enhanced after the modification with Ni-NGQDs (Figure 2a). In the presence of methanol, the photocatalytic activity of SiF/Ni-NGQD was considerably increased from 1.1 to 12.9 $\text{mmol g}^{-1} \text{h}^{-1}$ —which is the highest activity by Si-based photocatalysts to date (Table S2, Supporting Information)—with the increase of the Ni-loading from 0 to 2 wt.%. Further increasing the Ni content led to an obvious activity decrease, which could be attributed to the change of electronic structure such as the increase of O content and decrease of pyrrolic N configuration. These results demonstrate: i) the critical role of the Ni-doping that can provide greater and proper binding sites of reactants for oxidation and ii) a facile charge separation after the hybridization of SiF and Ni-NGQDs (Figure S13, Supporting Information).

Moreover, we attempted to perform photocatalytic biomass reforming and hydrogen production using SiF/Ni-NGQD1.4 under simulated sunlight irradiation. Instead of methanol, we tested small and macromolecular biomasses such as glucose, xylose,

Table 1. Comparison between the biomass photo-reforming.

| No. | Photocatalyst | Electron donor | Electrolyte | H ₂ [μmol g _{cat} ⁻¹ h ⁻¹] | Time [h] | Light source | Reference |
|-----|----------------|----------------|-------------------|---|----------|---|-----------|
| [0] | SiF | Cellulose | Water | 178 | 6 | Solar simulator [100 mW cm ⁻² , 1 sun] | This work |
| | SiF/Ni-NGQD | | (pH 7.0) | 5735 | | | |
| | SiF | Lignin | | 576 | | | |
| | SiF/Ni-NGQD | | | 14270 | | | |
| [1] | CNx/NiP | Cellulose | KPi (pH 4.5) | 1690 | 4 | Solar simulator [100 mW cm ⁻² , 1 sun] | [37] |
| | CNx/NiP | Lignin | KPi (pH 4.5) | 40.8 | 4 | | |
| | CNx/Pt | Cellulose | KPi (pH 7.0) | 4.1 | 24 | | |
| | CNx/Pt | Cellulose | 1 M KOH | 20.7 | 24 | | |
| | CNx/Pt | Cellulose | 10 M KOH | 44.6 | 24 | | |
| | CNx/Pt | Lignin | 10 M KOH | 14.6 | 24 | | |
| [2] | Pt/CdS/SiC | Cellulose | 10 M NaOH | 321.7 | 24 | Xe lamp [300 W] | [38] |
| | Pt/CdS/SiC | Lignin | 10 M NaOH | 11 | 24 | | |
| [3] | CdS/CdOx | Cellulose | 10 M KOH | 4400 | 18 | Solar simulator [100 mW cm ⁻² , 1 sun] | [26] |
| | CdS/CdOx | Lignin | 10 M KOH | 260 | 18 | | |
| [4] | Carbon dot/NiP | Galactose | Water (pH 6.0) | 159 | 24 | Solar simulator [100 mW cm ⁻² , 1 sun] | [29] |

cellulose, hemicellulose, and kraft lignin as electron sources (Figure 2b). We found that the SiF/Ni-NGQD1.4 can efficiently produce hydrogen, regardless of the type of the tested biomasses. In particular, when using kraft lignin, SiF/Ni-NGQD1.4 exhibited the highest efficiency of 14.2 mmol g⁻¹ h⁻¹, which was 25 times higher than that of the pristine SiF (Figure 2c). However, the photocatalytic activity of SiF/NGQD without Ni was significantly reduced (Figure S14, Supporting Information) probably due to a lower charge separation efficiency and fewer active sites (vide supra). The apparent quantum efficiencies (AQE) of SiF/Ni-NGQD1.4 at 400, 500, and 600 nm were 37%, 32%, and 26%, respectively (Figure 2d). To the best of our knowledge, SiF/Ni-NGQD exhibited the highest efficiency of solar hydrogen production with simultaneous photo-reforming of cellulose and lignin (Figure 2e and Table 1).^[26,29,37,38] It is noteworthy that we achieved the record-high efficiency using only earth-abundant and non-toxic elements under mild conditions (pH 7.0), while most conventional studies have been conducted using toxic CdS-based photocatalysts in harsh alkaline solutions (e.g., 10.0 M NaOH).^[26]

The hybrid photocatalyst SiF/Ni-NGQD1.4 maintained 98% of its initial photocatalytic activity even after five cycles of the photocatalytic test using lignin for 30 h, while the unmodified SiF maintained only 21% due to surface oxidation deactivating it (Figure 2f). Note that the oxidation of SiF led to the formation of Si-OH, which not only reduces the number of active sites but also acts as rapid recombination sites.^[39] TEM and XPS analyses showed that the ultrathin Ni-NGQD layer remained intact and prevented the SiF oxidation after 30 h of photocatalysis (Figure S15 and S16, Supporting Information). The protective role of Ni-NGQD against SiF oxidation was further confirmed by hydrogen evolution tests in 1.0 M KOH under dark conditions, where the oxidation and autonomous etching lead to the production of hydrogen (Figure S17, Supporting Information).^[40] These results consistently suggest that the Ni-NGQD layers act as a robust pro-

tection layer against the oxidation of SiF, as well as a charge separation and catalytic layer. We subsequently analyzed the oxidation byproducts of biomass upon photocatalytic hydrogen production. Particularly, we focused on the byproducts of kraft lignin because it is abundantly produced and can potentially be utilized as a feedstock of aromatic chemicals.^[41] Moreover, delignification and effective utilization of lignin are considered the most significant challenges for lignocellulosic biomass refinery.^[42] According to gas chromatography–mass spectrometry (GC-MS), photocatalytic reactions of lignin with the SiF/Ni-NGQDs resulted in the formation of lignin-derived phenolic compounds such as guaiacol, vanillin, and acetovanillone (Figure 3a,b). Similar to photocatalytic hydrogen production, the SiF/Ni-NGQD1.4 was superior to the pristine SiF for the efficient and selective depolymerization of lignin, demonstrating the role of Ni as an active site. The role of Ni-NGQD in oxidative biomass reforming was also confirmed by cyclic voltammetry (Figure S18, Supporting Information). Notably, 150 mg of vanillin—which is one of the most valuable byproducts from lignin—was produced from 1 g of lignin using SiF/Ni-NGQD1.4 (Figure 3b). The effective formation of vanillin and other phenolic products resulted from the improved specific cleavage of β-aryl ether linkages of lignin by SiF/Ni-NGQD1.4, as demonstrated in 2D ¹³C–¹H heteronuclear single-quantum correlation nuclear magnetic resonance (Figure 3c). No β-aryl ether linkages remained in the residual lignin when using SiF/Ni-NGQD1.4, whereas a significant portion remained when using the pristine SiF (Table S3, Supporting Information).

The selective photo-reforming of lignin by SiF/Ni-NGQDs was further confirmed by photocatalytic reactions of phenolic β-ether model dimer, guaiacylglycerol-β-guaiacyl ether (Figure 4a). During the photocatalytic conversion of the dimer under simulated solar irradiation, the cleavage of β-ether linkage was facilitated by SiF/Ni-NGQD1.4 (Figure 4b; Figure S19, Supporting

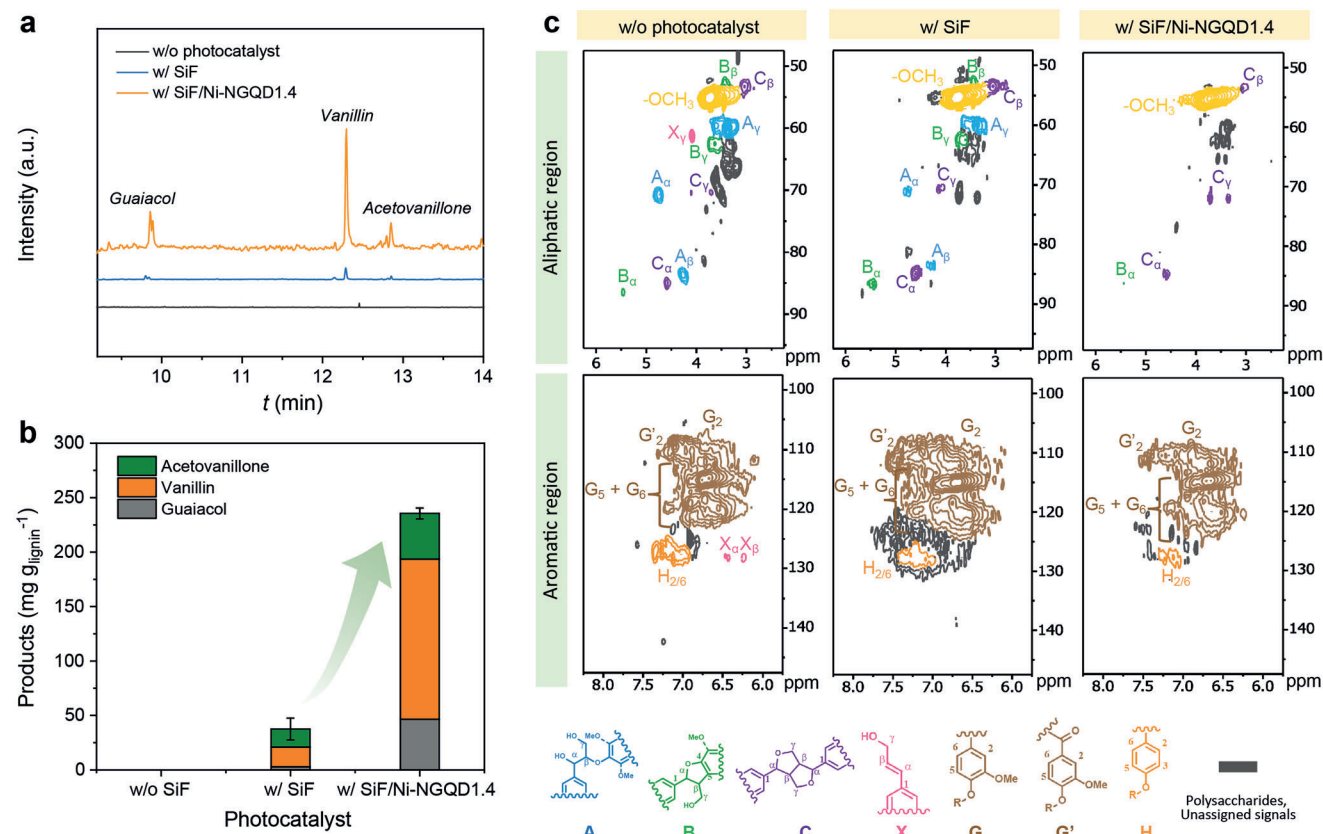


Figure 3. Photo-reforming of lignin depolymerization using SiF/Ni-NGQD photocatalysts. a) GC-MS spectra for the identification and quantification of the lignin byproducts after the irradiation of the simulated sunlight for 6 h. b) Comparison of the vanillin yield under various conditions. c) 2D NMR spectra of the residual lignin after the simulated solar irradiation for 6 h with and without photocatalysts.

Information). The SiF/Ni-NGQD1.4 was more efficient for the selective cleavage of β -aryl ether bond as well as C_{α} - C_{β} , allowing the photo-reforming of lignin to guaiacol and vanillin (Figure 4a,c).

In this study, we have demonstrated that SiF/Ni-NGQDs can enable efficient biomass reforming and hydrogen production under simulated solar irradiation. Despite abundance and low bandgap, Si-based photocatalysts have low stability and have been limited to reductive half-reactions such as HER. We have overcome such a big challenge by coating SiF with multifunctional Ni-NGQDs and employing oxidative biomass reforming instead of OER. The Ni-NGQDs not only facilitated the separation of photo-generated charge carriers but also improved the catalytic activity and stability of SiF for biomass photo-reforming. In principle, one can further investigate the effect of the size of SiF and Ni-NGQDs, and porosity of SiF on the photocatalytic performance of SiF/Ni-NGQDs as their photophysical properties, such as bandgap and band-edge positions, can be tailored according to their size^[43] and porosity.^[44] Of note, it was difficult to control the size and porosity of SiF in this study due to the inherent architecture of the SiF precursor, talc clay.^[36,39] While many conventional studies of biomass photo-reforming focused more on efficient hydrogen production and less on selective biomass photo-reforming, we achieved both efficient hydrogen production and selective biomass reforming. Furthermore, we utilized only earth-abundant and non-toxic elements, such as Si, Ni, C,

and N. However, it is noteworthy that the use of a dilute yet toxic HF solution is unavoidable in this study to remove native oxide layers to synthesize SiF. It is noteworthy that highly recalcitrant lignin was efficiently and selectively depolymerized into value-added chemicals under mild conditions without any strong acids and bases. However, further studies are required for practical application of SiF/Ni-NGQDs, such as more in-depth mechanism analysis, reactor designs, and separation of products.

3. Conclusion

We report light-driven biomass reforming and hydrogen production using Si-based hybrid photocatalysts under mild conditions. Low-bandgap SiF was modified with ultrathin layers of multifunctional Ni-NGQDs. The SiF/Ni-NGQDs not only exhibited the record-high photocatalytic activity for hydrogen production but also allowed the selective photo-reforming of lignin into value-added aromatic compounds, such as vanillin, under mild conditions. Moreover, SiF/Ni-NGQD photocatalysts can readily be recycled with a negligible performance degradation due to their heterogeneous nature and prevention of oxidation of Si by the Ni-NGQD layers. Our approaches can be applied in various energy conversion applications in coupling with biomass degradation.

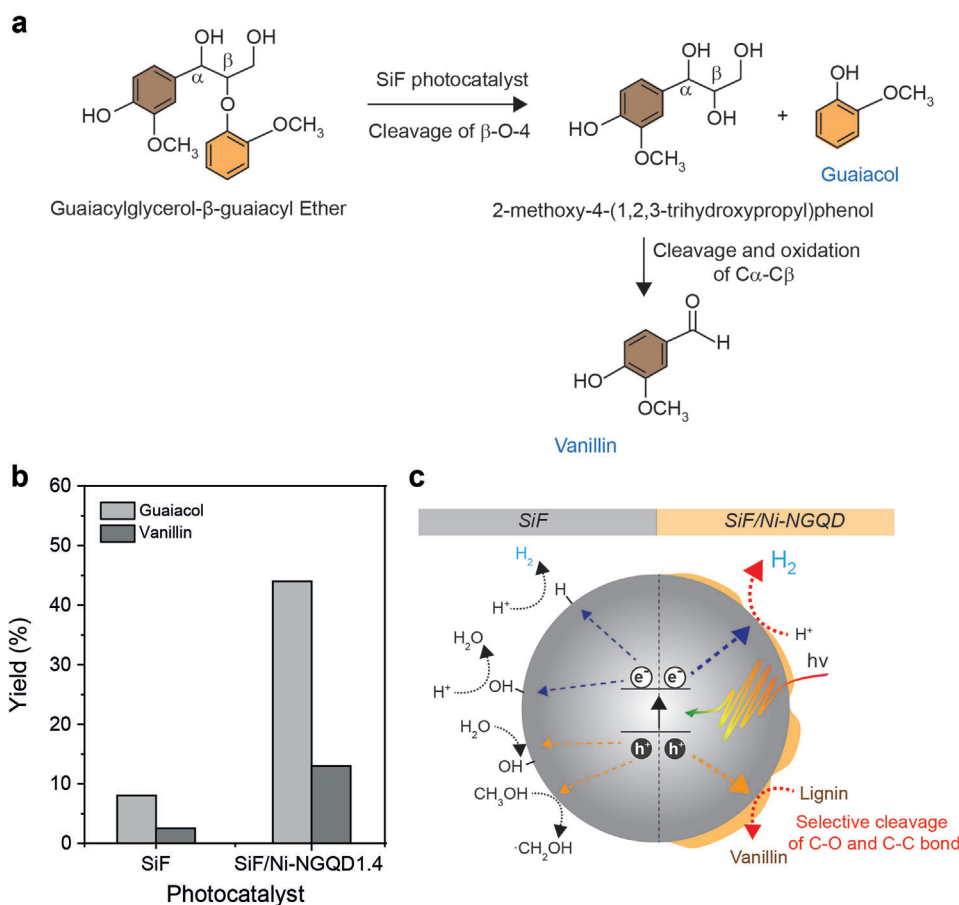


Figure 4. Selective cleavage of a lignin model compound using SiF-based photocatalysts. a) Schematic illustration of degradation of lignin model compound. b) Products after degradation of lignin model compound with SiF and SiF/Ni-NGQD 1.4. c) Schematic illustration of solar biomass reforming with SiF and SiF/Ni-NGQD.

4. Experimental Section

Synthesis of Ni-Coordinated Nitrogen-Doped Graphene Quantum Dots (Ni-NGQDs): To prepare Ni-NGQDs, 5 mg of tannic acid, 20 μ L of 2.0 M NaOH, and 20 μ L of ethylenediamine (0.03 mmol) were dissolved in 10 mL of deionized water under vigorous stirring. Then, different volumes (50, 100, 200, and 300 μ L) of 20 mM NiCl₂ were added to the solution, followed by a hydrothermal reaction at 190 $^{\circ}$ C for 6 h in a sealed Teflon-lined autoclave. After cooling to room temperature, the brown suspension was dialyzed (SpectraPore MWCO 1000) for 2 days to remove the salts and unreacted chemicals. In addition, NGQDs were synthesized in the absence of NiCl₂.

Preparation of Silicon Flake (SiF) and SiF/Ni-NGQD: SiF was prepared as in a previous report.^[36] In brief, SiF was prepared by magnesiothermic reduction of natural talc clay and a subsequent simple acid leaching process. First, commercially available natural talc clay was uniformly mixed with magnesium powder in a weight ratio of 1:0.8. The mixture was directly placed in a tube furnace and heated to 700 $^{\circ}$ C for 3 h in an argon atmosphere. After the reaction, the resulting powder was post treated in 1.0 M HCl and 0.5 wt.% HF solution respectively, to eliminate by-products including MgO and native oxide layers. For the preparation of SiF/Ni-NGQD, 20 μ L of 2 mg mL⁻¹ of Ni-NGQDs or NGQDs was added in 10 mL of water, and then 50 mg of SiF was added. After vigorous stirring for 30 min, the powder was collected, and dried under vacuum overnight.

Characterizations: The structure of NGQDs and Ni-NGQDs was characterized using XPS (K-alpha, Thermo Fisher) spectroscopy. The amounts

of Ni in Ni-NGQDs were determined using ICP-OES (700-ES, Varian). The morphology of Ni-NGQDs was examined using high-resolution TEM (JEOL, JEM-2100F, accelerating voltage of 200 kV). XRD analysis was used to check the formation of Ni nanoparticles (D/MAX2500V/PC, Rigaku). The absorption spectra of NGQDs and Ni-NGQDs were recorded using a UV-vis spectrophotometer (UV-2550, Shimadzu). The HOMO level of NGQDs, Ni-NGQDs, and SiF was evaluated using UPS (ESCALAB 250XI, Thermo Fisher). The morphology of SiF and SiF/Ni-NGQDs was examined using SEM (S-4800, Hitachi High-Technologies), high-resolution TEM, high-angle annular dark-field scanning TEM, and energy-dispersive X-ray spectroscopy (JEOL, JEM-2100F, accelerating voltage of 200 kV). The porous structure of SiF and SiF/Ni-NGQD was characterized by BET analysis (ASAP2420, Micromeritics Instruments). Finally, spectroscopic analyses of lignin before and after photocatalytic reaction were carried out with a VNMRs 600 nuclear magnetic resonance spectrometer (Agilent, USA). The size of NGQDs and Ni-NGQDs was determined using a zeta sizer (Nano ZS, Malvern).

Photocatalytic Hydrogen Evolution: The photocatalytic H₂ evolution tests were carried out with a 20 mL sealed vial. In brief, 5 mg of photocatalysts was added in 10 mL of deionized water containing the hole scavenger such as 10 wt% methanol, 10 mM glucose, 10 mM xylose, 10 mg of kraft lignin, 10 mg of cellulose, and 10 mg of hemicellulose. After purging with N₂ to remove O₂, the above reaction vessel was illuminated using a class AAA solar simulator (94023A, Newport) equipped with a 450 W Xe lamp and AM 1.5 G filter. Samples for GC analysis were collected from the headspace of a sealed vial using a gas-tight syringe and were analyzed

with a GC-2010 Plus gas chromatograph (Shimadzu Co., Japan). All photocatalytic tests were performed at least in triplicate for statistical analysis. The apparent quantum efficiency was evaluated using 300 W Xe lamp equipped with a CD130 monochromator (Newport Corporation, CA, USA) at 400, 450, 500, and 550 nm, respectively.

Extraction and Quantification of Byproducts after Lignin Photo-Reforming: A solution after lignin photo-reforming with Ni-NGQDs was filtered to remove insoluble aggregates and mixed with chloroform at a 1:1 volume ratio to extract aromatic compounds. Once phase separation occurred, 1 μ L of n-decane was added to 2 mL of the chloroform solution as an internal standard for GC-MS to identify and quantify aromatic compounds, such as vanillin and acetovanillone. GC-MS spectra were measured with a 450-GC gas chromatograph and a 320-MS mass spectrometer (Bruker, USA) equipped with an Rtx-5MS capillary column (30 m \times 0.25 mm \times 0.25 mm; Restek). Split injections (1 μ L) were performed with a GC Pal autosampler (CTC Analytics AG, Switzerland) at a split ratio of 25:1, using He as a carrier gas.

Supporting Information

Supporting Information is available from the Wiley Online Library or from the author.

Acknowledgements

Y.C. and S.C. contributed equally to this work. This work was supported by the grants (NRF-2021R1A2C2013684 and NRF-2022M3J1A1052840, to Jungki Ryu) through the National Research Foundation of Korea (NRF) funded by the Ministry of Science and ICT of Korea. This work was also supported by the Basic Science Research Program (NRF-2020R11A1A01057924, Y.C.) through the NRF funded by the Ministry of Education of Korea.

Conflict of Interest

The authors declare no conflict of interest.

Data Availability Statement

The data that support the findings of this study are available from the corresponding author upon reasonable request.

Keywords

biomass, graphene quantum dots, hydrogen evolution, photocatalysis, silicon

Received: February 18, 2023
Revised: March 27, 2023
Published online: June 5, 2023

- [1] Z. J. Han, R. Eisenberg, *Acc. Chem. Res.* **2014**, *47*, 2537.
- [2] K. Shimura, H. Yoshida, *Energy Environ. Sci.* **2011**, *4*, 2467.
- [3] A. Sartbaeva, V. Kuznetsov, S. Wells, P. Edwards, *Energy Environ. Sci.* **2008**, *1*, 79.
- [4] Y. J. Li, Y. J. Sun, Y. N. Qin, W. Y. Zhang, L. Wang, M. C. Luo, H. Yang, S. J. Guo, *Adv. Energy Mater.* **2020**, *10*, 1903120.

- [5] N. Kim, I. Lee, Y. Choi, J. Ryu, *Nanoscale* **2021**, *13*, 20374.
- [6] R. Ahorsu, M. Constanti, F. Medina, *Ind. Eng. Chem. Res.* **2021**, *60*, 18612.
- [7] N. Y. Du, C. Roy, R. Peach, M. Turnbull, S. Thiele, C. Bock, *Chem. Rev.* **2022**, *122*, 11830.
- [8] Z. P. Ifkovits, J. M. Evans, M. C. Meier, K. M. Papadantonakis, N. S. Lewis, *Energy Environ. Sci.* **2021**, *14*, 4740.
- [9] M. M. Abu-Omar, K. Barta, G. T. Beckham, J. S. Luterbacher, J. Ralph, R. Rinaldi, Y. Roman-Leshkov, J. S. M. Samec, B. F. Sels, F. Wang, *Energy Environ. Sci.* **2021**, *14*, 262.
- [10] S. J. Yim, H. Oh, Y. Choi, G. N. Ahn, C. H. Park, Y. H. Kim, J. Ryu, D. P. Kim, *Adv. Sci.* **2022**, *9*, 2204170.
- [11] A. W. Bartling, M. L. Stone, R. J. Hanes, A. Bhatt, Y. Zhang, M. J. Biddy, R. Davis, J. S. Kruger, N. E. Thornburg, J. S. Luterbacher, *Energy Environ. Sci.* **2021**, *14*, 4147.
- [12] T. Terlouw, C. Bauer, R. McKenna, M. Mazzotti, *Energy Environ. Sci.* **2022**, *15*, 3583.
- [13] J. Park, T. Kwon, J. Kim, H. Jin, H. Y. Kim, B. Kim, S. H. Joo, K. Lee, *Chem. Soc. Rev.* **2018**, *47*, 8173.
- [14] M. T. M. Koper, *Chem. Sci.* **2013**, *4*, 2710.
- [15] L. R. Lynd, G. T. Beckham, A. M. Guss, L. N. Jayakody, E. M. Karp, C. Maranas, R. L. McCormick, D. Amador-Nogues, Y. J. Bomble, B. H. Davison, C. Foster, M. E. Himmel, E. K. Holwerda, M. S. Laser, C. Y. Ng, D. G. Olson, Y. Roman-Leshkov, C. T. Trinh, G. A. Tuskan, V. Upadhyay, D. R. Vardon, L. Wang, C. E. Wyman, *Energy Environ. Sci.* **2022**, *15*, 938.
- [16] H. Oh, Y. Choi, C. Shin, N. V. T. Trang, Y. Han, H. Kim, Y. H. Kim, J. W. Lee, J. W. Jang, J. Ryu, *ACS Catal.* **2020**, *10*, 2060.
- [17] X. Wu, N. Luo, S. Xie, H. Zhang, Q. Zhang, F. Wang, Y. Wang, *Chem. Soc. Rev.* **2020**, *49*, 6198.
- [18] Y. Choi, R. Mehrotra, S.-H. Lee, T. V. T. Nguyen, I. Lee, J. Kim, H.-Y. Yang, H. Oh, H. Kim, J.-W. Lee, Y. H. Kim, S.-Y. Jang, J.-W. Jang, J. Ryu, *Nat. Commun.* **2022**, *13*, 5709.
- [19] W. Shang, Y. Li, H. Huang, F. Lai, M. B. Roeffaers, B. Weng, *ACS Catal.* **2021**, *11*, 4613.
- [20] Z. Xiang, W. Han, J. Deng, W. Zhu, Y. Zhang, H. Wang, *ChemSusChem* **2020**, *13*, 4199.
- [21] K. A. Davis, S. Yoo, E. W. Shuler, B. D. Sherman, S. Lee, G. Leem, *Nano Converg.* **2021**, *8*, 6.
- [22] H. Luo, J. Barrio, N. Sunny, A. Li, L. Steier, N. Shah, I. E. Stephens, M. M. Titirici, *Adv. Energy Mater.* **2021**, *11*, 2101180.
- [23] Y. K. Kho, A. Iwase, W. Y. Teoh, L. Madler, A. Kudo, R. Amal, *J. Phys. Chem. C* **2010**, *114*, 2821.
- [24] H. Zhao, X. Yu, C.-F. Li, W. Yu, A. Wang, Z.-Y. Hu, S. Larter, Y. Li, M. G. Kibria, J. Hu, *J. Energy Chem.* **2022**, *64*, 201.
- [25] G. Han, Y.-H. Jin, R. A. Burgess, N. E. Dickenson, X.-M. Cao, Y. Sun, *J. Am. Chem. Soc.* **2017**, *139*, 15584.
- [26] D. W. Wakerley, M. F. Kuehnel, K. L. Orchard, K. H. Ly, T. E. Rosser, E. Reisner, *Nat. Energy* **2017**, *2*, 17021.
- [27] X. Ning, G. J. N. Lu, *Nanoscale* **2020**, *12*, 1213.
- [28] X. J. Wu, S. J. Xie, H. K. Zhang, Q. H. Zhang, B. F. Sels, Y. Wang, *Adv. Mater.* **2021**, *33*, 2007129.
- [29] D. S. Achilleos, W. Yang, H. Kasap, A. Savateev, Y. Markushyna, J. R. Durrant, E. Reisner, *Angew. Chem., Int. Ed.* **2020**, *59*, 18184.
- [30] Z. Sun, Z.-H. Zhang, T.-Q. Yuan, X. Ren, Z. Rong, *ACS Catal.* **2021**, *11*, 10508.
- [31] Y. Choi, S. Bae, B.-S. Kim, J. Ryu, *J. Mater. Chem. A* **2021**, *9*, 13874.
- [32] M. A. Rahim, H. Ejima, K. L. Cho, K. Kempe, M. Mullner, J. P. Best, F. Caruso, *Chem. Mater.* **2014**, *26*, 1645.
- [33] Y. Li, Y. Wang, C.-L. Dong, Y.-C. Huang, J. Chen, Z. Zhang, F. Meng, Q. Zhang, Y. Huangfu, D. Zhao, *Chem. Sci.* **2021**, *12*, 3633.
- [34] D. M. Koshy, S. Chen, D. U. Lee, M. B. Stevens, A. M. Abdellah, S. M. Dull, G. Chen, D. Nordlund, A. Gallo, C. Hahn, *Angew. Chem., Int. Ed.* **2020**, *59*, 4043.

- [35] Y. Li, B. Liu, Y. Wang, S. Wang, X. Lan, T. Wang, *ACS Catal.* **2022**, *12*, 7926.
- [36] Y. J. Jang, J. Ryu, D. Hong, S. Park, J. S. Lee, *Chem. Commun.* **2016**, 52, 10221.
- [37] H. Kasap, D. S. Achilleos, A. Huang, E. Reisner, *J. Am. Chem. Soc.* **2018**, *140*, 11604.
- [38] H. Nagakawa, M. Nagata, *ACS Appl. Energy Mater.* **2020**, *4*, 1059.
- [39] J. Ryu, Y. J. Jang, S. Choi, H. J. Kang, H. Park, J. S. Lee, S. Park, *NPG Asia Mater.* **2016**, *8*, e248.
- [40] F. Dai, J. Zai, R. Yi, M. L. Gordin, H. Sohn, S. Chen, D. Wang, *Nat. Commun.* **2014**, *5*, 3605.
- [41] X. Shen, Y. Xin, H. Liu, B. Han, *ChemSusChem* **2020**, *13*, 4367.
- [42] Z. Huang, N. Luo, C. Zhang, F. Wang, *Nat. Rev. Chem.* **2022**, *6*, 197.
- [43] J. Peng, W. Gao, B. K. Gupta, Z. Liu, R. Romero-Aburto, L. H. Ge, L. Song, L. B. Alemany, X. B. Zhan, G. H. Gao, S. A. Vithayathil, B. A. Kaipparettu, A. A. Marti, T. Hayashi, J. J. Zhu, P. M. Ajayan, *Nano Lett.* **2012**, *12*, 844.
- [44] O. Bisi, S. Ossicini, L. Pavesi, *Surf. Sci. Rep.* **2000**, *38*, 1.